Journal of Solid State Chemistry 184 (2011) 3085–3094

Contents lists available at SciVerse ScienceDirect

Journal of Solid State Chemistry

journal homepage: www.elsevier.com/locate/jssc

Oriented $SrFe_{12}O_{19}$ thin films prepared by chemical solution deposition

Josef Buršík [a,*], Ivo Drbohlav [b], Zdeněk Frait [b], Karel Knížek [b], Radomír Kužel [c], Karel Kouřil [d]

[a] Institute of Inorganic Chemistry of the AS CR, v.v.i., 250 68 Husinec-Řež 1001, Czech Republic
[b] Institute of Physics of the AS CR, v.v.i., Na Slovance 2, 182 21 Praha 8, Czech Republic
[c] Charles University in Prague Faculty of Mathematics and Physics, Ke Karlovu 5, 121 16 Praha 2, Czech Republic
[d] Charles University in Prague, Faculty of Mathematics and Physics, V Holešovičkách 2, 180 00 Praha 8, Czech Republic

ARTICLE INFO

Article history:
Received 6 April 2011
Received in revised form
9 September 2011
Accepted 14 September 2011
Available online 22 September 2011

Keywords:
Hexagonal strontium ferrite
Chemical solution deposition
Epitaxial thin films

ABSTRACT

Thin films of $SrFe_{12}O_{19}$ (SrM) were prepared from a solution of iron and strontium alkoxides through the chemical solution deposition method on both amorphous (glassy SiO_2), and single crystal substrates (Si(100), Si(111), Ag(111), Al_2O_3(001), MgO(111), $MgAl_2O_4$(111), $SrTiO_3$(111)) substrates. The process of crystallization was investigated by means of powder diffraction, atomic force microscopy and scanning electron microscopy. Magnetization measurements, ferromagnetic and nuclear magnetic resonance were used for evaluation of anisotropy in the films. Whilst amorphous substrates enabled growth of randomly oriented SrM phase, use of single crystal substrates resulted in samples with different degree of oriented growth. The most pronounced oriented growth was observed on $SrTiO_3$(111). A detailed inspection revealed that growth of SrM phase starts through the breakup of initially continuous film into isolated grains with expressive shape anisotropy and hexagonal habit. A continuous film with epitaxial relations to the substrate was produced by repeating recoating and annealing.

1. Introduction

Strontium hexagonal ferrites $SrFe_{12}O_{19}$ (SrM) have a magnetoplumbite structure with an easy magnetocrystalline anisotropy axis along the *c* axis of the hexagonal unit cell. In bulk form they are commonly used for permanent magnets, in electro-acoustic devices, and are of great interest in thin film form for high density magnetic recording and millimeter-wave devices because of their large chemical resistivity, high permeability at high frequencies, and large uniaxial anisotropy [1–3]. In majority of these applications highly oriented films with *c*-axis perpendicular to the substrate are desirable. The films are in majority prepared by methods relying on cost expensive apparatus, such as sputtering [4], pulse laser deposition (PLD) [1,2,5], or liquid phase epitaxy (LPE) [6]. As a convenient alternative, chemical solution deposition (CSD) method can be used, thanks to the facts that it is simple, low cost, and can be rapidly developed for the evaluation of a new material system, and is amenable with standard semiconductor manufacturing methods. Using different types of organometallic precursors (alkoxides [7], ethyhexanoates [8], or nitrates [9]) and depending on the type of substrate (SiO_2 glass [7], polycrystalline alumina [8], or single crystal Al_2O_3 (001) [9]) either randomly [7,8] or oriented [9] ferrite films have been prepared through deposition by dipping or spinning. In order to obtain higher crystallinity and more pronounced anisotropy, it is necessary to do final crystallization at temperatures above 900 °C, where most of the substrates already react with material of ferrite film giving rise to either secondary phases ($Ba_xSi_yO_z$ [7]), or interdiffusion occurs ($BaAl_xFe_{12-x}O_{19}$ [5,7]). The aim of this work was to develop a procedure for preparation of highly oriented magnetically anisotropic hexagonal ferrite thin films by means of CSD method.

2. Materials and methods

In house synthesized alkoxides $Fe(OCHCH_2(CH_3)_2)_3$ and $Sr(OCH_2CH_2OCH_3)_2$ were used as metal precursors. Calculated amounts of $Fe(OCHCH_2(CH_3)_2)_3$ and $Sr(OCH_2CH_2OCH_3)_2$ (with 5% surplus in Sr to compensate its losses during annealing due to its reactivity with substrate) were dissolved in iso-butanol, mixed and heated for several hours to accomplish homogenization. Subsequently a suitable amount of 2,2-diethanolamine (DEA) used as a modifier (slowing down the reactivity and sensitivity towards air humidity) was added. All reactions and handling were done under dry nitrogen atmosphere to prevent reaction with air humidity and preliminary formation of strontium carbonate in solution. The concentration of this stock solution was $c=0.6$ M (Fe), the modifier molar ration was $n(DEA)/n(Fe)=1$. For the preparation of the thin "seed" layer, the stock solution was diluted to 0.1–0.3 M.

* Corresponding author. Fax: +420 220941502.
E-mail addresses: bursik@iic.cas.cz (J. Buršík), drbohlav@fzu.cz (I. Drbohlav), frait@fzu.cz (Z. Frait), knizek@fzu.cz (K. Knížek), kuzel@karlov.mff.cuni.cz (R. Kužel), Karel.Kouril@mff.cuni.cz (K. Kouřil).

0022-4596/$ - see front matter © 2011 Elsevier Inc. All rights reserved.
doi:10.1016/j.jssc.2011.09.024

Polished SiO_2 glass, Si(111), Si(100), Ag(111), Al_2O_3(001), MgO(111), $MgAl_2O_4$(111), $SrTiO_3$(100), and $SrTiO_3$(111) were used as substrates. They were cleaned by soaking in $KMnO_4$–H_2SO_4 mixture for 20 min, washing with deionized water and acetone, and finally dried in the flow of purified air. As-received Ag and MgO substrates were shortly washed with acetone and cleaned under flow of filtrated air just prior to deposition. The sols were filtered through 0.45 μm PTFE membrane filter unit just before the deposition. First of all, a thin film of SrM (20–40 nm of effective thickness) serving as a "seed" layer to promote the crystallization of "bulk" layer was deposited by spin-coating technique (RC8 Gyrset, KarlSuss) from diluted stock solution and crystallized at different temperatures. Then stock solution was used for spin-coating of the "bulk" layer. After drying at 110 °C for several minutes and pyrolysis of gel films at 450 °C for 15 min, crystallization annealing was done at temperatures in the range 500–1100 °C for 6 h in conventional tube furnace with temperature ramp 10 °C/min, under open air atmosphere. The deposition–annealing cycle was repeated eight times to obtain the desired film thickness.

Part of the starting precursor solution was converted into powder by drying at 110 °C for 24 h in air and used for DTA/TG coupled with mass spectrometry (Netzsch STA QMS 409), and high temperature XRD experiments (Bruker D8 powder diffractometer, MRI TC-wide range temperature chamber, Cu$K\alpha$1,2 radiation). The composition of solutions and thin films was checked by the volumetric titration and electron microprobe (Jeol JXA-733) analyses, respectively. Thickness of films was measured by a stylus apparatus (AlphaStep IQ KLA Tencor). The thickness of seed layer was calculated as a mean value gained on separately prepared sample composed of 10 crystallized "seed" layers. The thickness of final sample (seed layer+bulk layer) typically reached values around 600 nm for samples crystallized at 1100 °C. The thickness and composition were also evaluated from the SEM/EDAX analyses. SEM (Philips XL30 CP, Jeol JSM 6700 F NT) and AFM (Explorer, Thermomicroscopes, USA) analyses were used to evaluate microstructure of thin films. The room temperature $\theta-2\theta$ diffraction patterns of SrM films were measured on PANalytical XPert diffractometer (Cu$K\alpha$1,2 radiation, secondary graphite monochromator, PIXcel detector). Texture characterization and pole figure measurements were done by PANalytical XPert MRD diffractometer (Cu$K\alpha$1,2 radiation, polycapillary in the primary beam, the Eulerian cradle, parallel-plate collimator and secondary monochromator). Magnetization curves were measured at room temperature on SQUID (MPMS-5 S Quantum Design) apparatus. The microwave properties of SrM films were studied by ferrimagnetic resonance (FMR) measurements performed at room temperature, in reflection mode with external field applied normally to the sample plane, at frequencies 49 and 69 GHz using field modulation (ac field at 94 kHz) and lock-in amplifier technique [10]. Solid state ^{57}Fe NMR spectra were measured in a zero static external magnetic field using pulse coherent spectrometer Bruker Avance (equipped with homemade tunable probe head at temperature 4.2 K, with modified Carr–Purcell–Meiboom–Gill (CPMG) pulse sequence applied). The resulting frequency swept spectrum was evaluated as amplitude of the Fourier transform at excitation frequency.

3. Results

DTA/TG/MS measurements were used for optimization of drying, pyrolysis, and annealing regime. Results obtained on SrM powder prepared from dried precursor sol are shown in Fig. 1. It was observed that after the dehydration at 120 °C thermal degradation starts at temperatures ~250 °C with evolution of CO_2 and N_xO_y gases (detection of CO_2^+ and NO_2^+ fragments by MS) generating by burning out of metalloorganic precursor species and amine modifier (broad exotherm centered at 330 °C), accompanied by decrease in mass. The pyrolysis is finished at 450 °C, and above this temperature only minor mass decrease is observed. Though DTA curve did not show any endotherm at temperatures around 700 °C, two distinguishable bumps on DTG and MS curves located at 640 and 700 °C, respectively, can be assigned to decomposition of remaining $SrCO_3$ during the formation of SrM phase (compare with Fig. 2).

From high temperature XRD measurements (Fig. 2) it is evident that $SrCO_3$ formed already during drying at 110 °C, survives the pyrolysis and slowly disappears by reaction with iron precursor at temperatures slightly above 600 °C. The onset of

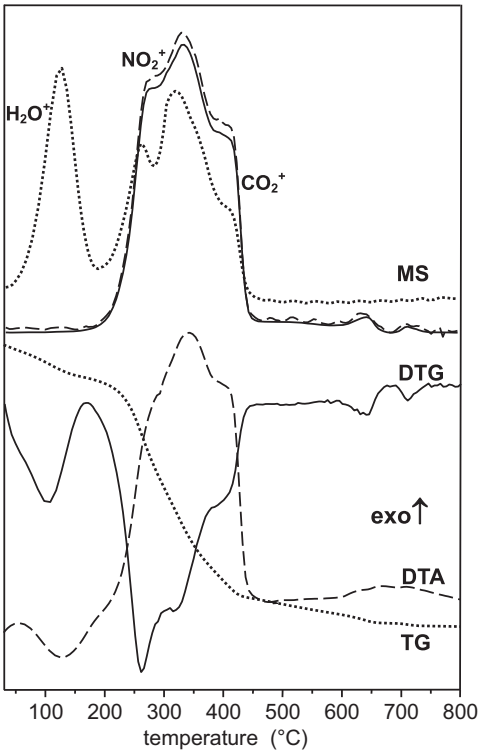

Fig. 1. DTA/TG/MS curves on dried $SrFe_{12}O_{19}$ sol measured in air.

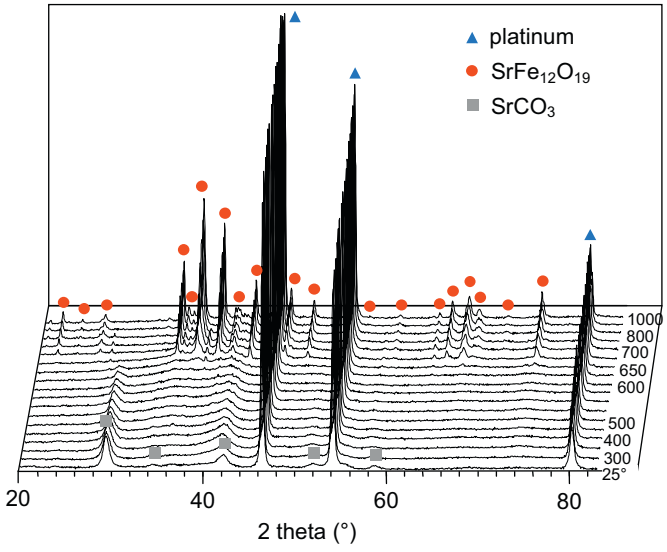

Fig. 2. High temperature powder diffraction patterns measured on powder from SrM precursor sol.

crystallization of SrM phase was found at 650 °C, where traces of α-Fe_2O_3, but not $SrCO_3$, were observed. At temperatures higher than 750 °C only pure ferrite phase was observed.

Fig. 3 shows the powder XRD patterns and Table 1 summarizes values of lattice misfit and experimental results about phase composition and degree of orientation of SrM thin films deposited on selected substrates. They were selected to include both amorphous and single crystal materials with both positive and negative misfit values. According to these results use of amorphous silica and silicon single crystals led to randomly oriented SrM phase for lower temperatures and to formation of $SrSiO_x$ and α-Fe_2O_3 phases due to enhanced reactivity of basic alkali earth with acidic Si at annealing temperatures above 900 °C. Use of substrates with even more convenient values of misfit – MgO(111) and $MgAl_2O_4$(111) – induced problems due to high reactivity of Mg^{2+} with Fe^{3+}. It was observed in case of MgO(111) substrate that randomly oriented SrM phase is formed below 800 °C and oriented $MgFe_2O_4$ spinel phases were obtained above this annealing temperature. Use of $MgAl_2O_4$(111) led to moderately oriented SrM phase (see Fig. 3(e)) for samples annealed at temperatures below 900 °C. In an effort to promote the orientation growth by rising further the annealing temperature weakly oriented $MgFe_2O_4$ spinel phase started to form. Use of Ag single crystal (not shown here) for orientation growth led to only randomly oriented SrM phase due to its low melting point (961 °C) and due to its relative softness making difficult for proper polishing of crystal surface. Al_2O_3(001) single crystal, which is otherwise commonly used for preparation of oriented hexagonal ferrites [1,2,9], led to only moderate orientation growth of SrM phase (not shown here) probably due to strong tendency of Al^{3+} for diffusion into ferrite structure where it substitutes for Fe^{3+} in ferrite structure.

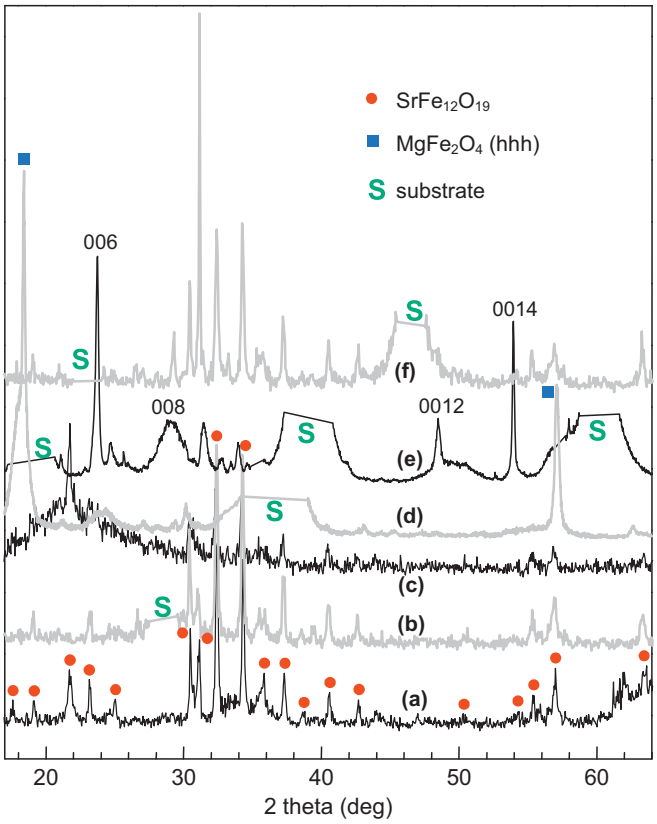

Fig. 3. θ–2θ powder diffraction patterns of SrM thin films deposited on different substrates (a) Si(100), (b) Si(111), (c) amorphous SiO_2, (d) MgO(111), (e) $MgAl_2O_4$(111), and (f) $SrTiO_3$(100) and annealed at 850 °C.

Diffraction pattern on SrM thin films deposited on $SrTiO_3$(100) substrate showed enhanced intensities of (00l) reflections for SrM phase evidencing certain degree of orientation growth. Well resolved reflections with indexes h, $k \neq 0$ observed in pattern imply presence of significant portion of nonoriented grains. By far the best orientation growth was observed with SrM deposited on $SrTiO_3$(111) single crystal substrate and results gained on this type of substrate will be subject of following paragraphs.

Fig. 4 shows the XRD pattern of SrM thin films deposited on $SrTiO_3$(111) substrate and annealed at different temperatures. It can be seen that samples are amorphous for temperatures lower than 550 °C. Annealing at 600 °C induces crystallization of randomly oriented SrM phase, which becomes preferentially oriented when temperature is increased to 700 °C as it is apparent from increasing intensity of 00l reflections. With further temperature increase up to 1100 °C this character of diffraction pattern becomes even more pronounced. Two of minority reflections can be ascribed to SrM phase (reflections 107 at 32.2° and 114 at 34.3°), there are no traces of the frequently noticed impurity phases, namely α-Fe_2O_3 and $Sr_xFe_yO_z$.

In order to semi-quantitatively assess the preferential growth, the so called ω scans (rocking curves) were measured on 008 reflection planes of SrM phase and are shown in Fig. 5 together with inset table containing their full width at half maximum (FWHM) values. According to these data the evolution of oriented growth starts at temperatures below 600 °C: layers annealed at 500 °C show random angular dispersion of [00l] directions. Samples annealed at 600 °C exhibit already sharp rocking curve

Table 1
Lattice misfits, phase composition, and orientation of $SrFe_{12}O_{19}$ thin films deposited on different substrates.

Substrate	Misfit (%) Δ_1 or Δ_2 [a]	Reactivity substrate↔SrM precursors	Phase composition of thin film
Si(111)	23.4 (Δ_1)	$t \geq 900$ °C:	$t \leq 900$ °C: random oriented SrM
Si(100)		$Sr \rightarrow SrSiO_x$	$t \geq 900$ °C: SrM+α-Fe_2O_3
SiO_2 amorph.	–	$t \geq 900$ °C:	$t \leq 900$ °C: random oriented SrM
		$Sr \rightarrow SrSiO_x$	$t \geq 900$ °C: SrM+α-Fe_2O_3
MgO(111)	1.35 (Δ_2)	$t \geq 800$ °C:	$t \leq 800$ °C: random oriented SrM
		$Fe \rightarrow MgFe_2O_4$	$t \geq 800$ °C: (111) oriented $MgFe_2O_4$
$MgAl_2O_4$(111)	−2.7 (Δ_2)	$t \geq 900$ °C:	$t \leq 900$ °C: (00l) oriented SrM
		$Fe \rightarrow MgFe_2O_4$	$t \geq 900$ °C: weakly (111) orient. $MgFe_2O_4$
Ag(111)	−1.8 (Δ_2)	m.p. (Ag)=961 °C	weakly (00l) oriented SrM, problems with polishing of single crystal surface
Al_2O_3(00l)	−6.0 (Δ_1)	$t \geq 900$ °C:	moderately (00l) oriented SrM
		$Al \rightarrow Sr(AlFe)_{12}O_{19}$	
$SrTiO_3$(100)	−6.5 (Δ_2)	$t \leq 1200$ °C:no reaction	$t \geq 900$ °C: (00l) oriented SrM
$SrTiO_3$(111)	−6.5 (Δ_2)	$t \leq 1200$ °C:no reaction	$t \geq 700$ °C: strongly (00l) oriented SrM

[a] $\Delta_1 = (a(substr) - a(SrM)/a(substr)) \times 100$, $\Delta_2 = (\sqrt{2}a(substr) - a(SrM)/\sqrt{2}a)substr)) \times 100$

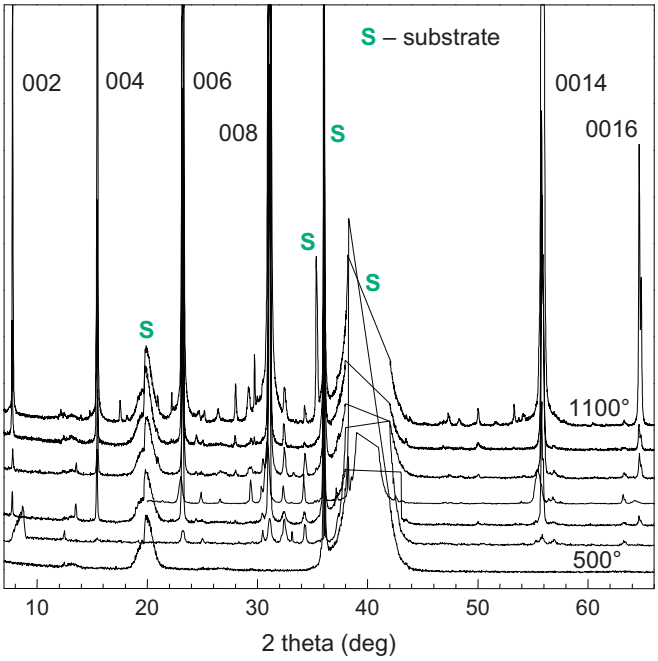

Fig. 4. θ–2θ powder diffraction patterns of SrM thin films deposited on $SrTiO_3$(111) substrate and annealed in air at different temperatures.

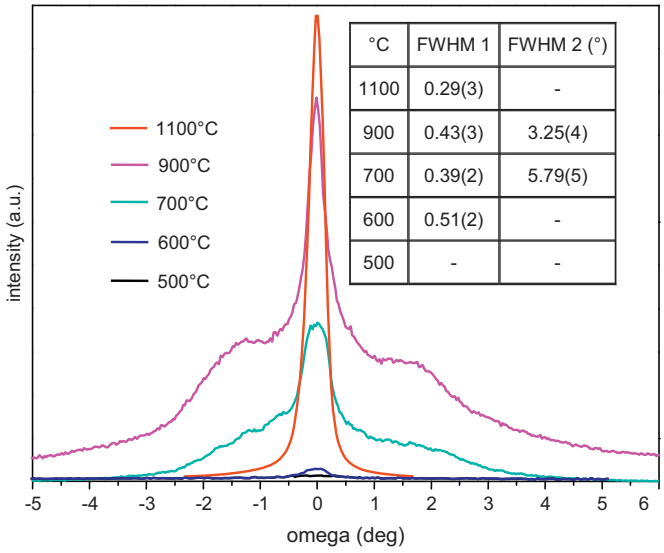

°C	FWHM 1	FWHM 2 (°)
1100	0.29(3)	-
900	0.43(3)	3.25(4)
700	0.39(2)	5.79(5)
600	0.51(2)	-
500	-	-

Fig. 5. Diffraction rocking (ω) curves measured on 008 reflection of SrM thin films deposited on $SrTiO_3$(111) substrate and annealed in air at different temperatures.

with FWHM=0.51°. With increasing temperature the rocking curves change their shape further. Samples crystallized in temperature range from 600 to 900 °C exhibited bimodal shape of its rocking curves. We fitted these complex curves as being composed of two components: over the broad hump having FWHM values between 3° and 6°, a second much sharper peak with FWHM values below 0.5° is overlaid. We speculate that the second narrow peak is due to crystallites adjacent to bottom "seed" layer that were "eaten" by well oriented crystallites from seed layer during the grain growth progressively occurring with increase in annealing temperature. The first broader peak can come from grains located in upper layers, where lower degree of orientation is reached for temperature interval 700–900 °C. Continual decrease of FWHM values for this peak with increase in

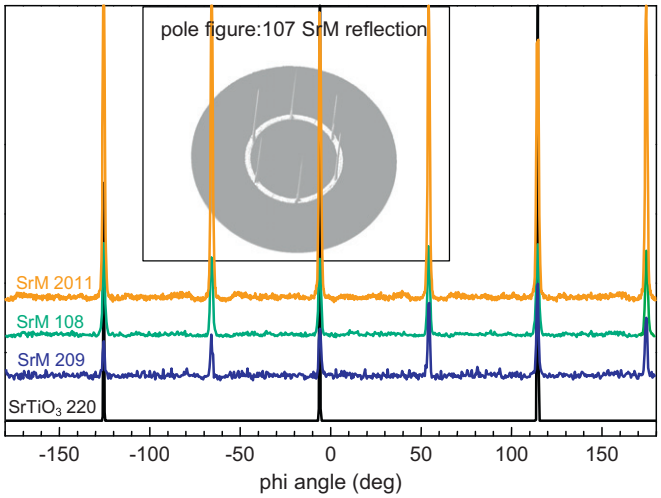

Fig. 6. Diffraction ϕ scans and pole figure (nested) measured on 107 reflection of SrM thin films on SrM film deposited on $SrTiO_3$(111) and annealed in air at 1100 °C.

temperature indicates that in population of less oriented grains improvement in orientation progressively continues. Above 1000 °C only narrow mono modal rocking curve with FWHM less than 0.3° was measured indicating high degree of alignment of c-axis parallel to the substrate normal. Fitting was done with either single or double Gaussian function without any correction taking into account divergence of irradiated area from exact focusation plane.

In order to examine a possible epitaxy, we probed additional Bragg reflections in nonspecular directions. Fig. 6 shows the so called Φ scans measured on 108, 209, and 2011 reflections of SrM phase (and also on 220 reflection of $SrTiO_3$(111) substrate). It can be seen that three maxima (from six maxima separated by 60° obtained for ($h0l$) planes of SrM phase) coincide with three maxima of the substrate (exhibiting 3-fold symmetry of (111) plane view). The six fold symmetry of azimuthal Φ scans and their matching to the substrate reflects the true epitaxial nature of the film. The distributions of the in-plane film and substrate orientations are sharply peaked with their FWHM reaching values 1.3° (2011), 1.4° (209), 1.5° (108), and 0.5° (220) for thin film and substrate Φ scans, respectively. The same six fold symmetry has been observed on pole figures measured on 107 reflection of SrM phase as it is illustrated by inset in Fig. 6. The orientation relation between the SrM and $SrTiO_3$(111) can then be characterized as being (001)SrM//(111)$SrTiO_3$ and [100]SrM//[110]$SrTiO_3$.

The evolution of surface morphology of SrM layer on $SrTiO_3$(111) substrate examined by AFM is shown in Figs. 7–9. Starting with low crystallization temperatures the surface is composed of closed packed equiaxed particles with size less than 10 nm forming smooth surface (Fig. 7(a)). At 700 °C these equiaxed particles start to coalescence in needle-like grains with the aspect ratio of about 10:1, protruding about 70 nm above the level of surrounding grains (the root mean square (r.m.s.) surface roughness values increase from 3.7 nm to more than 25 nm for 800 °C, Fig. 7(b) and (c)).

With further increase of annealing temperature to 900 °C these needle-like grains change their shape from elongated to circular hemispherical with the size of about 400 nm at their base and forming faceted surface (Fig. 8(a)). At 1000 °C the grains increase their size at the expense of their flattening (Fig. 8(b)). Some crystallites start to acquire habits of regular hexagons with well developed facets and reaching heights about 40 nm. The development of hexagonal shape continues further with increase in temperature. After crystallization at 1100 °C the fully developed

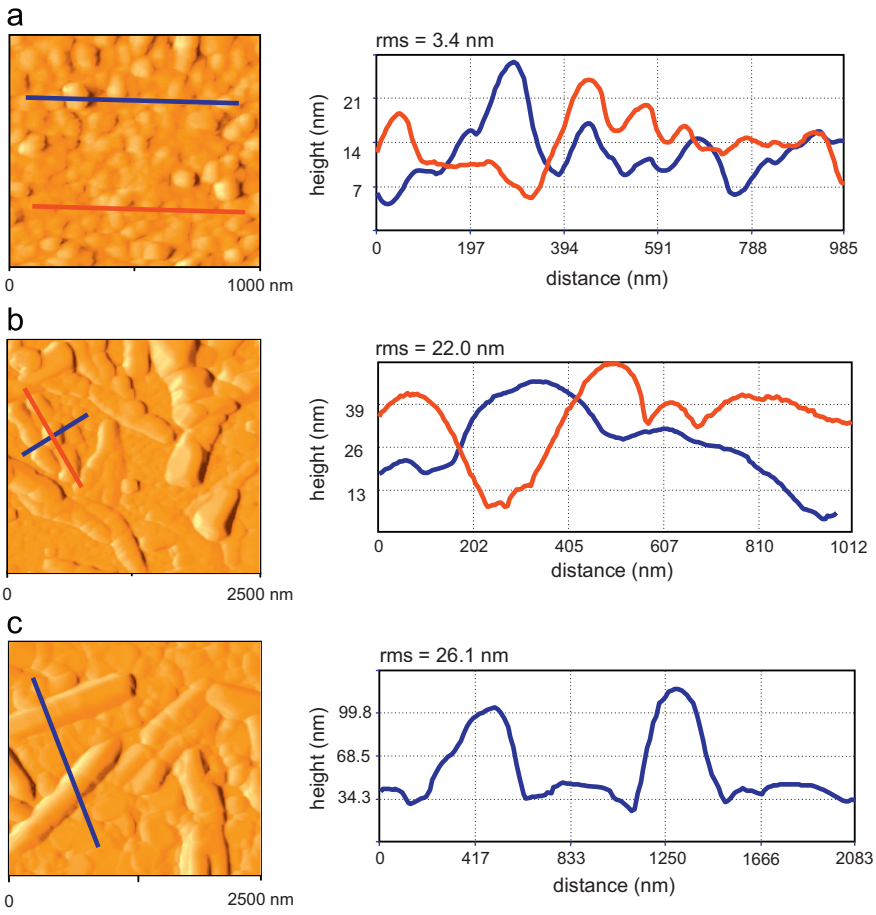

Fig. 7. AFM images of "seed" SrM layer deposited on $SrTiO_3$(111) and crystallized at 600 (a), 700 (b) and 800 °C (c), together with height profile scans over selected features in surface and calculated r.m.s. values.

hexagonal grains become isolated and reach size of about 600 nm and heights of about 50 nm above the base level (Fig. 8(c)). Because of the observed hexagonal growth habit of crystallites and powder diffraction measurements (not shown here) that confirmed epitaxial relation between islands and substrate, it was concluded that the seed layer crystallized at 1100 °C possesses the required characteristics for the growth of oriented films. With further increase of temperature to 1200 °C (Fig. 9(a)) the hexagonal grains start to coalescence forming very large grains but at the same time small droplet are formed due to some melting process causing degradation of hexagons. At 1300 °C the melting led to complete deterioration of hexagons (Fig. 9(b)). Fig. 9(c) exhibits typical microstructure of the surface after the deposition of bulk 600 nm thick layer onto the 40 nm thick seeding layer, both crystallized at 1100 °C.

The microstructure of SrM thin films inspected by means of SEM is shown in Fig. 10. Annealing at temperatures slightly higher than the onset of SrM phase crystallization induces formation of film microstructure of equiaxed grains with size below 50 nm including certain porosity (Fig. 10(a)). Increasing the annealing temperature causes the transformation of crystallites from equiaxial to platelets with length of about 300–400 nm and thickness less then 100 nm (Fig. 10(b)) that are randomly oriented throughout the cross-section of the film. By further increase in annealing temperature (cross-section view not shown here) the platelets start to sinter changing grainy microstructure into more compact one, losing its original appearance of well resolved grains. The process of sintering is illustrated in Fig. 10(c) and (d), displaying plane view of surface of SrM film crystallized at 1100 °C before (Fig. 10(c)), and after (Fig. 10(d)) the removal of the surface layer by means of ion etching. According to Fig. 10(c) the surface of 600 nm thick film is composed of thin platelets of hexagonal shape oriented mostly parallel to the surface with basal diameter about 1000 nm, frequently with their bases glued-up together and forming stacking microstructure. Removal of top surface by ion etching uncovers the interior of the film (Fig. 10(d)). The microstructure looks like being composed of continuous mass without any grainy structure and incorporates certain porosity indicating incomplete sintering.

Fig. 11 shows the static magnetic properties of SrM thin films on $SrTiO_3$(111) crystallized at 800 °C (Fig. 11(a)) and 1100 °C (Fig. 11(b)) measured with orientation of external magnetic field both parallel, and perpendicular to the sample surface. The data in Fig. 11(a) give broad hysteresis loops with a coercive field of 6–7 kOe, a remanent magnetization of 110–130 emu/cm^3, and a saturation magnetization of approximately 200 emu/cm^3 for both orientations of magnetic field. The data collected on samples crystallized at 1100 °C (Fig. 11(b)) give for perpendicular orientation square shaped hysteresis loop with a coercive field 2.8 kOe, a remanent magnetization 220 emu/cm^3, and a saturation magnetization of 230 emu/cm^3. Parallel orientation of magnetic field has been observed as almost linear response of magnetization versus field and reduced hysteresis character of the loop. Our films are *c*-axis oriented with pronounced magnetic anisotropy and reach magnetic parameters, which are consistent with values on SrM ferrite in literature. The static magnetization data were used to determine the saturation magnetization for fields used in ferromagnetic resonance measurements.

Fig. 12 shows the differential absorption dA/dH vs. external field H for 600 nm thick SrM film deposited on $SrTiO_3$(111) and

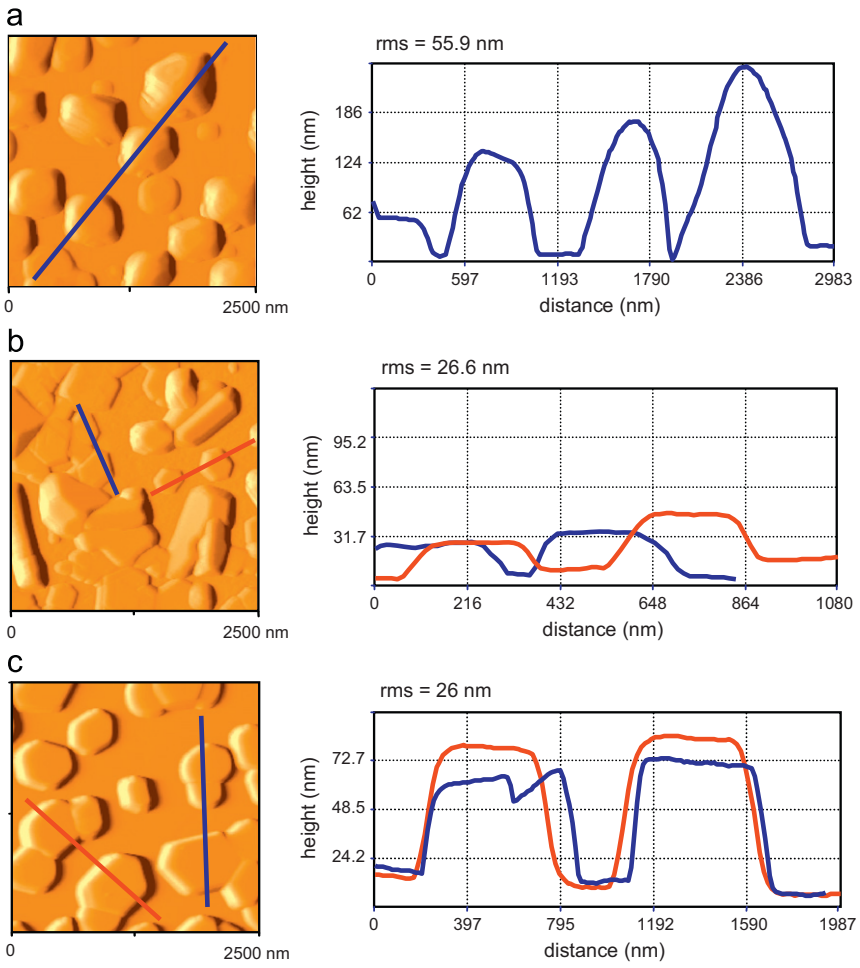

Fig. 8. AFM images of "seed" SrM layer deposited on $SrTiO_3$(111) and crystallized at 900 (a), 1000 (b) and 1100 °C (c), together with height profile scans over selected features in surface and calculated r.m.s. values.

crystallized at 800 °C (Fig. 12 (bottom)), and at 1100 °C (Fig. 12 (top)). For fields above saturation magnetization field and in case of material exhibiting preferential growth with c axis collinear with sample normal, resonance frequency is given by the following equation [11]:

$$\omega_{res} = \gamma(H_{res} - H_{demag} + H_A) = g\frac{\mu_B}{h}\left(H_{res} - 4\pi M_{sat} + \frac{2K_A}{M_{sat}}\right)$$

where ω_{res} is the resonance frequency, γ is gyromagnetic ratio, H_{res} is resonance external field, H_{demag} is demagnetization field, H_A is anisotropy field, μ_B is the Bohr magneton, K_A is uniaxial anisotropy constant, and g is the g-factor. Using the values of saturation magnetization M_{sat} from magnetization SQUID measurements and by performing FMR measurements at least at two frequencies we can obtain the values of parameters g and K_A.

Sample crystallized at 800 °C did not exhibit saturation field value for fields needed for resonance at both 49 and 69 GHz (see Fig. 11(a)), and show broad resonance curve widths at both frequencies in Fig. 12 (bottom); therefore the g-value 1.991 found for sample crystallized at 1100 °C was used for the evaluation of spectra of both samples. Then we have obtained for sample crystallized at 800 °C for both working frequencies H_A=15.9 kG and K_A=1.46 erg/cm^3 (Fig. 12 (bottom)). The sample crystallized at 1100 °C exhibits narrower FMR curves at both frequencies (Fig. 12 (top)), the values of anisotropy field H_A and anisotropy constant K_A were evaluated as 16.5 kG and 1.88 erg/cm^3, respectively.

The ^{57}Fe NMR spectrum measured on the film samples crystallized at 800 and 1100 °C together with inset plots of fitted line profiles are plotted in Fig. 13. The four spectral lines corresponding to resonance of ^{57}Fe nuclei in 12k, 4f_1, 2a and 4f_2 sites of $SrFe_{12}O_{19}$ magnetic structure [12,13] (the 2b resonance was not measured because of suspected too low signal/noise ratio) are plotted as shifted from resonant frequencies observed in bulk single crystal [13]. In comparison to the spectrum of a bulk SrM single crystal it is evident that the spectral lines of magnetic sublattices with magnetization parallel to total magnetization (12k and 2a, spin 'up') are shifted to higher frequencies, while the lines of sublattices with antiparallel magnetization (4f_1 and 4f_2, spin 'down') are shifted to lower frequencies. Shift of lines found for the sample crystallized at 800 °C are markedly (about 0.2 MHz) higher relatively to sample crystallized at 1100 °C. While the line shifts of sample 800 °C are nearly uniform, in case of sample crystallized at 1100 °C the shift of 2a line is lower than those of the remaining lines. In addition, the lines are significantly broadened, having the linewidth of approximately 0.4 MHz (corresponding to width of the distribution of magnetic field being about 0.3 T), which is more than an order of magnitude higher than in the single crystal. Spectral shapes were fitted to the experimental data supposing the same line profile for all the four detected lines, of course considering the mirror symmetry of the 12k and 2a lines with respect to those of 4f_1 and 4f_2. The lines in case of the sample crystallized at 1100 °C were asymmetric, while the Gaussian profile was sufficient for fitting spectrum of the sample crystallized at 800 °C. Integral intensities of individual

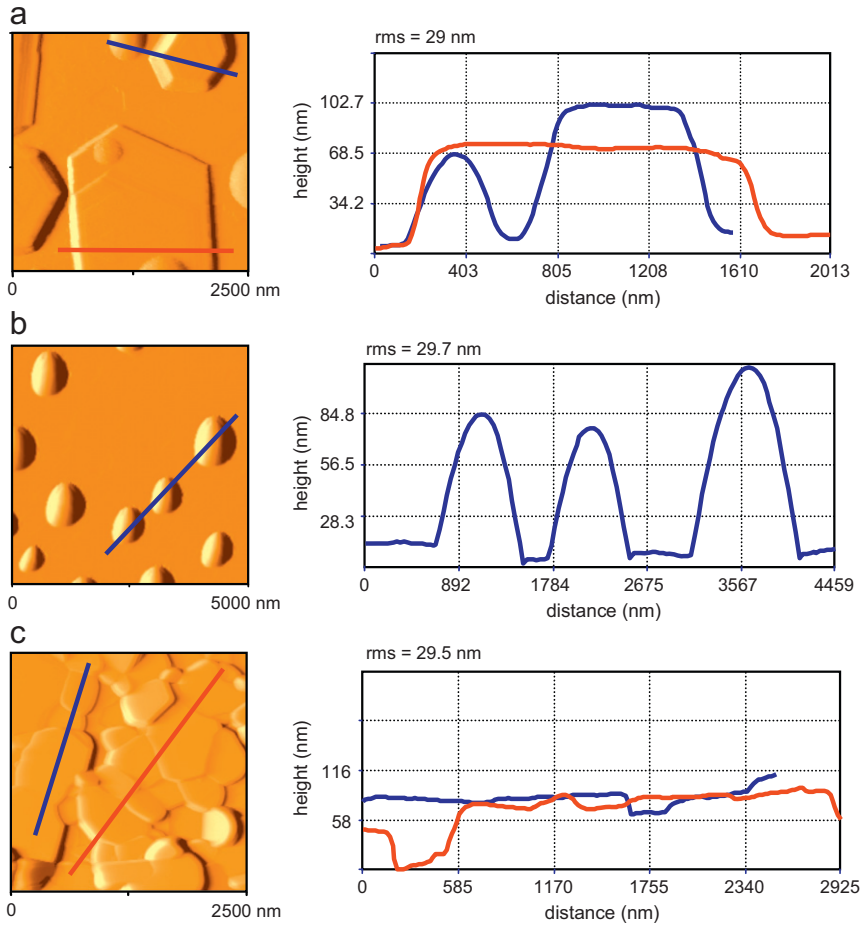

Fig. 9. AFM images of "seed" SrM layer (a, b) crystallized at 1200 °C (a), 1300 °C (b); and top surface of "bulk" layer (c) crystallized at 1100 °C (both seeding and bulk layer), all deposited on $SrTiO_3$(111), together with height profile scans over selected features in surface and calculated r.m.s. values.

resonance lines obtained from the fit well correspond to multiplicities of underlying sites.

4. Discussion

To obtain single phase thin film, optimization of preparative conditions must be achieved. In our case, two effects emerged as potentially hazardous in an attempt to prepare good quality films: destruction of film microstructure due to uncontrolled evolution of combustion products during pyrolysis of gelled films, and an incomplete decomposition of alkali earth carbonates before the onset of crystallization of ferrite phase. Thus, the heat treatment regime has been scheduled based on DTA/TG and high temperature XRD measurements, so that the pyrolysis has been conducted at rather higher temperature 450 °C with 15 min delay which enabled complete removal of organics from the film. The process of crystallization in SrM thin films has been studied starting with annealing temperature of 600 °C where most of the $SrCO_3$ is already decomposed and crystallization of ferrite phase starts (see Figs.1 and 2).

In most of the reports on oriented hexagonal thin films, single-crystal Al_2O_3(001) (e.g. [1,2]) or MgO(111) (e.g. [5,8]) substrates were used in combination with some physical deposition method. Although films deposited onto substrates with different symmetry or large value of lattice misfit, or amorphous substrates would not intuitively be expected to be oriented, results published [4,14,15] has exhibited certain degree of *c*-axis oriented growth of hexagonal ferrite onto amorphous SiO_2 with ZnO buffer layer by PLD [15], and on Si(100) and YSZ(100) by laser ablation method [4,14]. Regarding the in-plane orientation of ferrite films no direct experimental evidence is given in these papers.

Our attempt to grow oriented SrM thin films on selected group of substrates by means of CSD method illustrate commonly accepted fact that for the same type of material–substrate arrangements different preparation techniques can give thin film with different properties. Generally, using our "chemical" method we observed randomly oriented SrM phase for temperatures at which the onset of orientation growth is usually observed using "physical" deposition methods (typically 800–900 °C [1,2,4,5,14,15]). Increasing the annealing temperature above 900 °C caused frequent formation of films with better *c*-axis orientation but at the same time noticeable smearing of film–substrate boundary accompanied by interdiffusion or formation of other phases occurred (see Table 1). This effect can be observed also by comparing the values of FMR line widths (see Fig. 12) where higher annealing temperature leads to pronounced narrowing of the line width (the value of the anisotropy field changes only slightly). The reason for this can lie among others in the difference, in which both types of methods deliver thermal energy to atoms needed for them to undergo oriented growth due to their increased mobility: continuous deposition of adatoms on concurrently preheated substrates in e.g. PLD experiments is more convenient than use of post-deposition pyrolysis and annealing typical for CSD methods. Seeing our findings about phase composition of thin films prepared on different substrates summarized in Table 1, conclusion can be drawn that not only structural similarity and low lattice misfit between deposit and substrate are substantial for reaching of

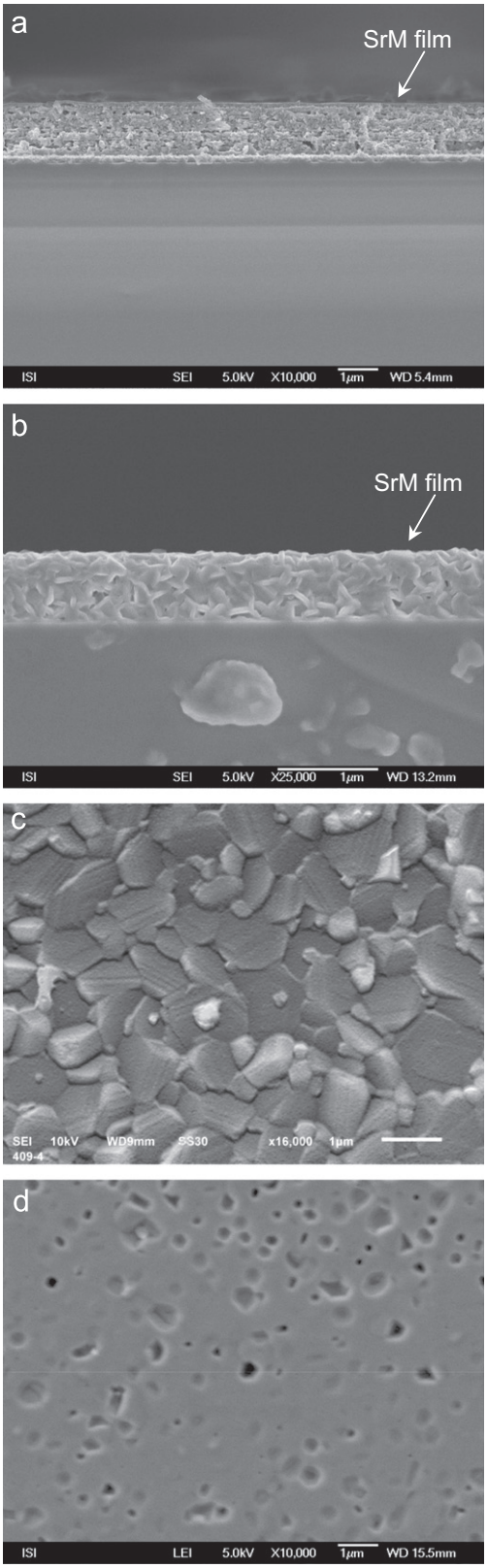

Fig. 10. Cross-section (a, b) and plane view (c, d) SEM images of the SrM thin film deposited on $SrTiO_3$(111) and crystallized at 700 °C (a), 900 °C (b), and 1100 °C (c,d) before (c) and after (d) the ion etching of the surface.

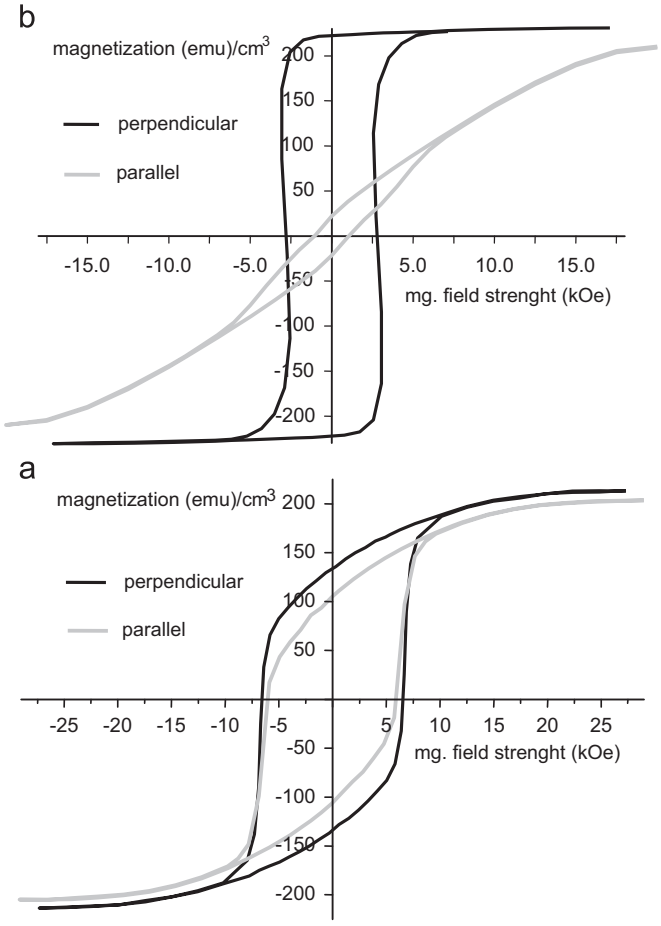

Fig. 11. Magnetization hysteresis curves measured at room temperature on SrM thin films deposited on $SrTiO_3$(111) and crystallized at 800 °C (a), and 1100 °C (b), with both parallel and perpendicular orientations of mg. field relatively to thin film surface.

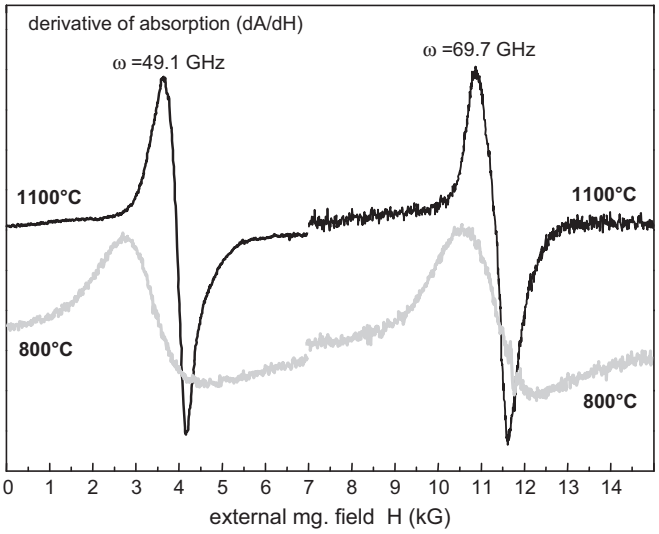

Fig. 12. FMR absorption derivative (dA/dH) vs. static external field (H) spectra of thin SrM films deposited on $SrTiO_3$(111), crystallized at 800 °C (bottom) and 1100 °C (top), and measured at room temperature at 49.1 and 69.7 GHz.

oriented growth. It is evident by comparison of phase composition gained on substrate with far the best lattice misfit value and appropriate symmetry relation (MgO(111), with results gained on substrate with almost five times higher value of lattice misfit ($SrTiO_3$(111)), or phase composition gained on otherwise commonly used Al_2O_3(001) substrate, with results on $SrTiO_3$(111) substrate exhibiting almost the same value of lattice misfit, that

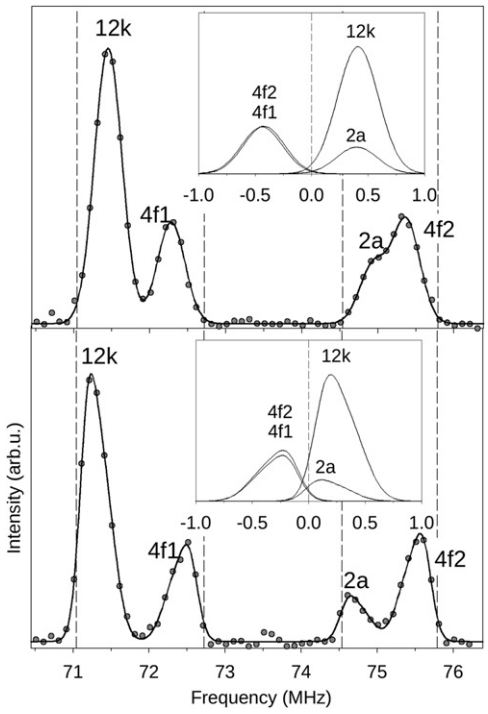

Fig. 13. ^{57}Fe NMR spectra of SrM thin films deposited on $SrTiO_3$(111) and crystallized at 800 °C (top) and 1100 °C (bottom). Circles—experimental data, solid line—fit. Vertical dashed lines are drawn at resonance frequencies corresponding to perfect single crystal. Nested plots: fitted shape and shifts of spectral lines from resonant frequencies in a single crystal sample.

also chemical reactivity of constituent elements at elevated temperatures is of importance.

X-ray diffraction data of θ–2θ scans and rocking curve scans on films deposited on $SrTiO_3$(111) substrate (Figs. 4 and 5) illustrate, that the process of oriented growth starts almost simultaneously with the onset of phase crystallization (i.e. at approximately 600 °C) and continues further with increase in annealing temperature. Rocking curve measurements (Fig. 5) enable us to speculate about this development. The flat curve of SrM films annealed at 500 °C (the contribution from the seeding layer to total measured signal was indiscernible) indicate almost random orientation of grains. Rocking curve measured on sample annealed at 600 °C showing quite narrow distribution of [001] directions and relatively lower intensity indicates that the orientation growth commences. We believe that this process proceeds in bottom-up manner through the consumption of fine, randomly oriented grains by large epitaxial grains from seeding layer that possess a low interfacial energy and act as nucleation sites for the growth of oriented films as it is described in literature [16–18]. The driving force for this transformation should be the reduction in excess grain boundary energy [17]: larger well oriented grains at the bottom interface consume smaller poorly oriented grains above. We consider the bimodal shape of rocking curves observed for samples annealed at temperatures between 700 and 900 °C (centered at the same ω, and with progressively increasing significance of the narrow peak and diminishing contribution of broad component to the envelope curve) to be the consequence of incompleteness of this transformation. After annealing at temperatures above 1000 °C, fully transformed highly oriented film showing monomodal and very narrow rocking curves is obtained and epitaxial relationship between substrate and thin film was proved (see Fig. 6).

Two types of sample surfaces were studied by means of AFM: surface of the 40 nm (effective thickness) seed layer and top surface of the 600 nm thick final sample (Figs. 7–9). The measurements on the first type of sample proved that under optimum conditions isolated islands of grains having a hexagonal shape with basal plane oriented parallel to the film surface are formed. Usage of this phenomenon for getting better oriented films has been described for variety of oxide systems: $Zr(Y)O_2$ on Al_2O_3 (001) [16], $PbTiO_3$ on $SrTiO_3$(111) [17], $PbTiO_3$ on $LaAlO_3$(100) [18] or $SrTiO_3$, $BaTiO_3$ on $LaAlO_3$(100) [19].

In order to be the "trick" of using a thin seed layer for the oriented growth effective, the deposited layer must be sufficiently thin to form a discontinuous layer of in nature isolated grains with an epitaxial relation to the substrate to allow for the elimination of nonoriented grains and simultaneously the coverage should be sufficient to have sufficiently high number of these seeds [17]. These isolated, single crystal islands with an epitaxial relation are the configuration that has the lowest free energy when the film thickness is less than a certain critical value [16,17]. By recoating the substrate covered with seed layer, the seeds consume much smaller nonoriented or poorly oriented grains within the new deposits through grain growth occurring with increasing annealing temperature as it can be illustrated in Fig. 5 by decreasing FWHM values of the broad texture component for bimodal rocking curves observed at intermediate temperatures. Based on XRD texture analysis and AFM measurements it was determined that optimum conditions for growing of seed layer is 40 nm effective thickness and crystallization at 1100 °C.

According to SEM measurements, the microstructure changed from finely grained equiaxed grains observed in sample annealed at 700 °C (Fig. 10(a)) to the films composed of needle-like shaped grains with entrapped porosity in sample annealed at 900 °C (Fig. 10(b)). Comparing these results with XRD data on films (see Fig. 4) and with rocking curve measurements (Fig. 5) we can conclude, that despite the use of epitaxial seed layer, (homogeneous) nucleation still can occur within the bulk of the film. Similar findings were mentioned by other authors [19–21]. They argue that either the thermal energy barriers for hetero- and homo-nucleation (which differ in factor governed by contact angle [20]) are not dramatically different, or the decomposition pathway from amorphous pyrolysed material leading to the formation of relatively stable intermediates within the film dictates the final microstructure. The negative influence of reaction pathway on microstructure and orientation development during the annealing has been confirmed for systems where one of the constituent elements was alkali earth metal giving rise to relatively stable carbonates. It was found in [21] that even under almost optimal conditions, when $BaTiO_3$ epitaxial seed layer of high quality was prepared by means of molecular beam epitaxy, the formation of nonoriented crystallites within the bulk of film dominates microstructure in $BaTiO_3$ upper films deposited by CSD. Similarly, in [19] the crystallization of $SrTiO_3$ and $BaTiO_3$ thin films on $LaAlO_3$ substrates using seeded growth, bulk nucleation was observed instead of nucleation starting at the seeding layer with following consumption of an amorphous matrix lying upwards. It is believed that in all these cases the decomposition pathway takes place via intermediate carbonate which form at temperatures between 300 and 400 °C and undergo decomposition by reaction with other constituent at temperatures around 600 °C [19,20]. Our results for the retarded decomposition of $SrCO_3$ observed in dried sol by means of high temperature XRD (Fig. 2) are apparently in agreement with those studies.

The removal of material from top surface of films heat treated at 1100 °C (Fig. 10(c and d)) demonstrate that beneath the surface of densely packed thin platelets of hexagonal shape the microstructure collapsed into a more compact microstructure losing its original appearance of well resolved grains. Though, certain porosity is still observed, evidencing incomplete sintering.

The static magnetic measurements (Fig. 11) essentially confirmed the findings of the structural and microstructural studies. The decrease in coercive field for the external field applied perpendicular to sample plane from 6.5 kOe (annealing at 800 °C) to 2.8 kOe (annealing at 1100 °C), together with pronounced squareness (M_{rem}/M_{sat} ratio) reaching value 0.97 for sample annealed at 1100 °C, indicate improved magnetic anisotropy with increase in annealing temperature. The presence of certain hysteresis for data measured with parallel orientation (Fig. 11(b)) is related to domain considerations and is indicative of presence of various types of defects (point defects, off-stoichiometric materials, dislocations, stacking faults, etc.) all of which can influence the sample response to external magnetic field during magnetization.

Results of FMR measurements confirmed that our g-factor and anisotropy field H_A values are comparable with values obtained for films prepared by PLD method ($g=1.99\pm0.01$ measured in [21], and H_A around 17 kG found in [6,22,23]). However, in general, our CSD films exhibit broader linewidths compared with PLD films (see [21–23], where some samples yield line widths around 30 Oe for only $BaFe_{12}O_{19}$).

One can perceive the common NMR lineshape as proportional (by the ^{57}Fe gyromagnetic ratio) to distribution of projection of the demagnetizing fields throughout the sample to local easy axis. The maximal possible value of demagnetizing field induced ^{57}Fe NMR lineshift in SrM is about 0.9 MHz (corresponding to isolated single domain grain with demagnetizing factor $N=4/\pi$). The observed lineshifts are much lower, despite the fact, that as seen by SEM, the grains are very oblate. This is due to compensation of demagnetizing fields via interaction between grains. The lineshifts of sample annealed at 1100 °C are further reduced—the oriented grains, have better potential to compensate internal field within the film, furthermore, since the lateral dimensions of grains are about 1 μm, domain walls may be formed, thus contributing to the reduction as well. Not perfectly uniform lineshifts in sample crystallized at 1100 °C indicate, that mechanism other than macroscopic field contributes to resulting spectrum. Additional effects could bring along slight modification of electronic structure, which would alter hyperfine field in each iron site differently. Strain or structural defects are the most probable candidates.

5. Conclusion

This study has shown that single phase, epitaxial $SrFe_{12}O_{19}$ thin films can be prepared by chemical solution deposition method on $SrTiO_3$(111) single crystal substrates using seeding layer composed of high density of well-oriented, isolated SrM grains. These well-oriented seeds were formed by the breakup of polycrystalline, finely grained layer prepared under optimum deposition and heat treatment conditions. By overcoating this seeding layer, epitaxial $SrFe_{12}O_{19}$ thin films was obtained, with pronounced crystallographic and magnetic anisotropy as shown by XRD, SQUID and FMR and NMR measurements. Nevertheless, the problem of homogeneous nucleation of unoriented grains was not totally avoided as it was indicated by SEM and XRD measurements. Samples crystallized at 1100 °C gave values for in-plane and out-of plane coercivity fields 1.1 and 2.8 kOe, respectively, with M_{rem}/M_{sat} ratio reaching value 0.97 for out of plane orientation. Relatively higher values of FMR linewidth prepared can be attributed to strains due to higher crystallization temperatures and film-substrate lattice misfit used in this work. The strains may be as well responsible for nonuniform NMR lineshifts in sample crystallized at 1100 C. To improve magnetic characteristics of ferrite films, several approaches will be tested: development of a more suitable buffer layer, changes in annealing conditions to avoid formation of stable alkali earth carbonates. Work on these is currently under progress.

Acknowledgments

This work was supported by the Grant Agency of Academy of Sciences of the Czech Republic under Grant nos. IAA100100803 and MS0021620834. The authors would like to thank to M. Maryško (IoP) for SQUID measurements, P. Bezdička and A. Petřina (IIC) for powder XRD θ–2θ and rocking curve measurements, M. Maříková (IIC) for DTA measurements, F. Míka (ISS Brno) for SEM measurements and H. Štěpánková (FMP CU) for helpful discussions on NMR results.

Appendix A. Supplementary Information

Supplementary data associated with this article can be found in the online version at doi:10.1016/j.jssc.2011.09.024.

References

[1] S.R. Shinde, S.E. Lofland, C.S. Ganpule, S.B. Ogale, S.M. Bhagat, T. Venkatesan, R. Ramesh, J. Appl. Phys. 85 (1999) 7459.
[2] Y.-Y. Song, S. Kalarickal, C.E. Patton, J. Appl. Phys. 94 (2003) 5103.
[3] G. Albanese, A. Deriu, The Landolt–Börnstein Database, Group III Condesed Matter, vol. 4b, Part B, Chapter 10, Springer Verlag, Eds. K.-H. Hellwege, A.M. Hellwege, 547.
[4] B.R. Acharya, S. Prasad, N. Venkataramani, S.N. Shringi, R. Krishnan, J. Appl. Phys. 79 (1996) 478.
[5] S.A. Oliver, I. Kozulin, M.L. Chen, C. Vittoria, Appl. Phys. Lett. 76 (2000) 3612.
[6] S.G. Wang, S.D. Yoon, C. Vittoria, J. Appl. Phys. 92 (2002) 6728.
[7] J. Buršík, Z. Šimša, M. Čerňanský, J. Sol-Gel Sci. Technol. 8 (1997) 947.
[8] D.F. Ryder, J.H. Fenstermacher, J. Am. Ceram. Soc. 73 (1990) 282.
[9] H. Tang, W. Zhang, B. Peng, W. Zhang, Thin Solid Films 518 (2010) 3342.
[10] Z. Frait, Czech. J. Phys. 9 (1959) 403.
[11] J.R. Macdonald, Proc. Phys. Soc. 64 (1951) 968.
[12] H. Štěpánková, J. Englich, P. Novák, D. Sedlák, M. Pfeffer, Hyperfine Interact. 50 (1989) 639.
[13] H. Štěpánková, K. Kouřil, V. Chlan, P. Görnert, R. Müller, J. Štěpánek, J. Magn. Magn. Mater. 322 (2010) 1323.
[14] V. Papakonstantinou, M.O. ONeill, R. Atkinson, I.W. Salter, R. Gerber, J. Magn.Soc. Jpn. 20 (1996) 333.
[15] P.C. Dorsey, C. Vittoria, J. Magn. Magn. Mater. 137 (1994) 89.
[16] K.T. Miller, F.F. Lange, J. Mater. Res. 6 (1991) 2387.
[17] A. Seifert, A. Vojta, J.S. Speck, F.F. Lange, J. Mater. Res. 11 (1996) 1470.
[18] J.H. Kim, F.F. Lange, J. Mater. Res. 14 (1999) 1626.
[19] R.W. Schwartz, P.G. Clem, J.A. Voight, E.R. Byhoff, M. van Stry, J. Headley, N.A. Missert, J. Amer. Ceram. Soc. 82 (1999) 2359.
[20] R.W. Schwartz, Chem. Mater. 9 (1997) 2325.
[21] M.C. Gust, N.D. Evans, L.A. Mamoda, M.L. Mecartney, J. Amer. Ceram. Soc. 80 (1997) 2828.
[22] C.A. Carosella, D. Chrisey, P. Lubitz, J.S. Hotwitz, P. Dorsey, R. Seed, C.J. Vittoria, Appl. Phys. 51 (1992) 5107.
[23] L.V. Saraf, S.E. Lofland, A.V. Cresce, S.M. Bhagat, R. Ramesh, Appl. Phys. Lett. 79 (2001) 385.